

Extended High-order Disturbance Observer based Clutch Actuator Model Uncertainty Estimation of Ball-ramp Dual-clutch Transmission

Dong-Hyun Kim and Seibum B. Choi, *Member, IEEE*, (e-mail: kkddh@hyundai.com).

Abstract—The Ball-ramp dual-clutch Transmission (BR-DCT) was proposed to overcome the disadvantages of conventional DCT. Specifically, BR-DCT is designed to reduce the amount of clutch actuator energy consumption and reverse torque during tie-up, in which two clutches are engaged simultaneously. Additionally, since the self-energizing principle is used, the actuator model can be used without the friction coefficient, which is the main uncertainty of the clutch actuator. These features can greatly contribute to enhancing the shift control performance of the BR-DCT. However, the measurement error due to friction between actuator parts causes a small amount of uncertainty. In this paper, a method using Extended High-Order Disturbance Observer (EH-DOB) is proposed to estimate this uncertainty. The EH-DOB used in the proposed method guarantees convergence even in a system in which the gain of the disturbance is time-varying. The convergence of the estimation error was verified through proof of the proposed algorithm. Experimental verification of the proposed algorithm was performed using a test bench that simulates a powertrain equipped with BR-DCT. As a result, it was confirmed that the uncertainty estimation result using EH-DOB showed high accuracy. As a result, it was verified that the uncertainty estimation method using the proposed algorithm has high accuracy and stability enough to perform disturbance rejection control.

Index Terms—Dual-clutch transmission, DCT, Ball-ramp, Self-energizing, Uncertainty estimation, Nonlinear disturbance observer, DOB, High-order DOB.

I. INTRODUCTION

IN the past few decades, fast and smooth shifting to improve ride comfort and fuel efficiency has become the ultimate goal of automotive powertrain control research [1], [2]. Various types of transmissions have been developed to achieve this goal. The development of all transmissions is based on Manual Transmission (MT). MT has excellent power transmission efficiency because it uses a clutch that can transmit power directly through friction [3]–[5]. In addition, the price is low, the size is small, and no shift controller is required. However, MT requires a lot of manipulation by the driver, and shift speed and shock may increase depending on the driver's driving ability [6].

To compensate for these shortcomings of MT, Automated Manual Transmission (AMT) was developed [7]. AMT is

designed to shift using a clutch actuator, which reduces the complexity of MT operation and compensates for shift control performance changes according to driving ability. However, the shifting time is still slow and shift shock may occur due to the uncertainty of the clutch friction coefficient. In addition, because MT and AMT use a single clutch, they have a common disadvantage: a torque interruption phenomenon occurs when the driving torque becomes zero during shifting [8].

To address this, Clutch to Clutch (C2C) transmissions [9] such as Automatic Transmission (AT) and Dual-Clutch Transmission (DCT) have been developed [10], [11]. C2C transmission uses the method of crossing the off-going clutch with the on-coming clutch after selecting the gear of the shaft of the clutch to be shifted to in advance. Therefore, it is possible to inherit the advantages of AMT, which does not require the driver's operation and has constant shift control results regardless of the driver; it is also possible to reduce shift time. However, because C2C transmission crosses the torque between the two clutch shafts connected to one final gear, if the engaged clutch is not fully released, a tie-up phenomenon in which both clutches are engaged may occur [8]. If a tie-up phenomenon occurs during shifting, oscillation may increase the shift shock as well as incur breakage of the clutch shaft. To prevent tie-up, AT used a torque converter (a type of fluid coupling) as a power transmitting device. Because torque is transmitted using fluid, the gear selecting clutches is usually slipped rather than locked up. Therefore, AT is possible to eliminate the tie-up phenomenon and shift quickly and smoothly without precise shift control. However, the low transmission efficiency of the torque converter was the main reason for limiting the maximum torque and reducing the fuel efficiency of vehicles using AT [11], [12]. In addition, AT requires torque measurement for clutch torque control but is not equipped with a torque sensor due to cost, durability, and space constraints. In the end, it can be estimated using the clutch actuator model, but the accuracy of the clutch actuator model decreases due to the change in the clutch friction coefficient, making it difficult to estimate the clutch torque. As a result of this, it is difficult for AT to improve the performance of clutch torque control. In addition, because it uses several planetary gear sets and clutches, AT is larger in size and has a higher manufacturing cost compared to MT.

To address these limitations of AT, DCT replaces the torque converter with a dual-clutch to increase maximum transmission torque and fuel efficiency. In addition, gear selector

Seibum B. Choi is Professor at the School of Mechanical, Department of Mechanical Engineering, at the Korea Advanced Institute of Science and Technology (KAIST), 291 Daehak-ro, Yuseong-gu, Daejeon 305-338, Republic of Korea (e-mail: sbchoi@kaist.ac.kr).

Dong-Hyun Kim is Senior Research Engineer in R&D Division, Hyundai Motor Company, 150 HyundaiYeonguso-ro, Namyang-eup, Hwaseong-si, Gyeonggi-do, 18280, Republic of Korea

actuators are installed as in AMT. In general, DCT is designed as one clutch in which even gears are connected, and another clutch in which odd gears are connected. Therefore, it can be considered that two AMTs are combined. The DCT uses a shifting method that crosses the torque of the on-coming clutch and the off-going clutch. Therefore, torque interruption does not occur during shifting [13]. In this way, DCT has the advantages of high transmission efficiency of AMT and fast and convenient shifting of AT [9]. In addition, it can be manufactured in sizes similar to those of MT or AMT, and the manufacturing cost is lower than that of AT. However, because it is mainly manufactured as a normally open type for fail-safety, the amount of energy consumed by the clutch actuator to maintain the clutch engagement is large. As a result of this, DCT has a theoretical fuel efficiency improvement effect of 30% compared to AT, whereas the actual fuel efficiency improvement effect is only 15% [14]. In addition, the shift shock tends to increase when clutch tie-up occurs during shifting due to the absence of a torque converter. Therefore, it is necessary to reduce shift shock by preventing tie-up through precise clutch torque control. The difficulty of measuring clutch torque as in AT still limits the clutch torque control performance.

Various studies have been conducted to compensate for the shortcomings of DCT. First, to reduce the amount of energy consumed by the clutch actuator of the DCT, DCT applying the self-energizing principle was studied [15], [16]. In both studies, the clutch actuator energy consumption was mechanically improved by using a rack-pinion type self-energizing mechanism. The rack-pinion clutch system uses the principle that the clutch actuator pushes the release bearing and creates the rotational force of the pinion gear through a lever. In this process, clutch torque acts as mechanical feedback to the actuator due to the self-energizing principle of the rack-pinion mechanism, thereby obtaining an additional engagement force. However, the nonlinearity due to backlash and friction of the gears reduces clutch slip control performance and energy efficiency. To address these drawbacks of rack and pinion DCT, Ball-ramp DCT (BR-DCT) was developed [17], [18]. BR-DCT reduces the amount of energy consumed by the clutch actuator by using a self-energizing effect such as rack and pinion DCT. However, the nonlinearity of gears was eliminated by using a ball and ramp mechanism. Because the ball-ramp mechanism does not require a minimum size of the gear teeth, it can be designed with a smaller volume than the rack and pinion mechanism. If the transmission is designed with a small volume, it can be expected to improve fuel efficiency due to weight reduction.

Second, BR-DCT could also reduce the tie-up effect, which is a disadvantage of conventional DCT. If using the direction of the self-energizing effect varies according to the direction of the clutch torque, the actuator engagement force of the BR-DCT can be adjusted according to the direction of the clutch torque. Using this feature, it is possible to reduce the reverse torque when a tie-up occurs.

Third, unlike conventional DCT, a friction coefficient is removed from the clutch actuator model. Conventional DCT uses a clutch torque model using a friction coefficient, so

actuator model uncertainty may occur due to a change in friction coefficient, which may cause deterioration of shift performance. However, since BR-DCT uses a model from which the friction coefficient has been removed, (that is, a clutch torque model expressed only by the position and force of the actuator.) more accurate input calculation is possible. In this way, the BR-DCT can improve the performance of shift control. However, a small amount of actuator model uncertainty still occurs due to a measurement error according to the mounting position of the force sensor. This measurement error has a smaller effect than the change in the friction coefficient of the conventional DCT, but must be estimated to improve the shift control performance.

The modeling error of the BR-DCT clutch actuator is similar to the change in the friction coefficient of the conventional DCT. Therefore, it is necessary to examine the research on model uncertainty estimation of conventional DCT [19]–[21]. In general DCT, the modeling error of the actuator is mainly caused by the change of friction coefficient of the clutch disk. The friction coefficient of the clutch disk changes with the temperature, torque, and slip speed of the clutch. This uncertainty can be measured through the torque sensor of the clutch. However, a typical DCT is not equipped with a torque sensor and the BR-DCT is the same. Therefore, it is necessary to estimate the model uncertainty. To solve this problem, various studies using state/disturbance observer or parameter adaptation have been performed. First, estimating input uncertainty using an unknown input observer was used [19]. In this method, the uncertainty of the actuator is expressed as a lumped disturbance of the clutch torque and estimated by the observer. However, even though the dominant uncertainty is a change in the friction coefficient since the lumped disturbance of the clutch torque is estimated, it is estimated including the known value. In other words, there was a limit in estimation accuracy because it was not possible to distinguish between known and unknown information. Second, a method using parameter adaptation was studied [20]. In this method, a nominal friction coefficient is specified, and the constant value change of the friction coefficient is assumed based on that value. This value was estimated by parameter adaptation. Compared to [19], this method can slightly increase the estimation accuracy by composing a disturbance only with unknown information. However, since the change of the friction coefficient during shift control varies rapidly depending on slip speed and temperature, it is inappropriate to estimate the constant. Third, an uncertainty estimation with a disturbance observer (DOB) was used [21]. However, since it is assumed that the disturbance is constant, it is not significantly different from adaptation. After all, the above studies commonly estimated the change in friction coefficient by defining it as slow varying uncertainty. This method was suitable when uncertainty was close to constant but was not suitable for rapidly changing situations.

Unlike the conventional DCT, actuator modeling error of BR-DCT includes friction between components and model change of lever. Friction is most of the model uncertainty, which is caused by the mounting issue of the force sensor. This uncertainty can be analyzed as the measured result as shown

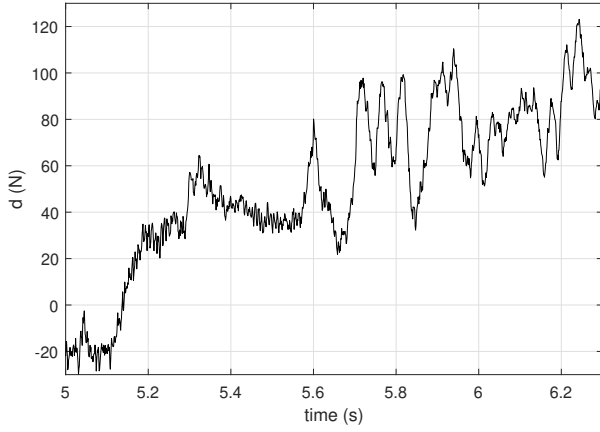


Figure 1. The actual value of the disturbance was measured using a torque sensor installed for verification.

in Fig. 1, and it can be seen that it changes with time during shift control. From these analysis results, it is inappropriate to estimate slow varying uncertainty such as adaptation or constant DOB. In addition, nonlinearity exists because the self-energizing mechanism is modeled. Therefore, in this paper, the DOB using the nonlinear technique is used as a method to estimate the uncertainty of the clutch actuator model. In addition, the powertrain model is used together as in previous studies to increase the estimation performance.

To estimate uncertainty, various nonlinear DOBs classified according to the characteristics of the disturbance were investigated. As the easiest method, a nonlinear constant DOB can be used for estimation of a relatively slow disturbance [22]. However, using a constant DOB to estimate fast varying disturbances reduces the convergence rate of the estimation. To address this, harmonic nonlinear DOB has been studied [23]. To apply harmonic DOB, the number of nodes and coefficients of the Fourier transform of disturbance is required. That is, it is suitable when the type of disturbance is known to some extent. However, since the uncertainty of BR-DCT is different for every shift, only limited information can be used. To reflect this characteristic, a high-order DOB (H-DOB) that uses only the maximum order when the disturbance is expressed as a polynomial can be used [24], [25]. The H-DOB assumes that the disturbance is polynomial and uses a DOB design method using only the maximum order. Also, the convergence rate of disturbance estimation can be adjusted using the characteristic polynomial. In addition, when a polynomial disturbance of H-DOB is expressed as Linear Time-Invariant (LTI), it can be expressed as one type of harmonic DOB. In this case, H-DOB can be directly applied to BR-DCT because of its polynomial expression of disturbance and its structure targeting a nonlinear system. Therefore, it is suitable as a nonlinear DOB for estimating the disturbance of BR-DCT. [26]

However, there is a problem in estimating the uncertainty of BR-DCT using H-DOB. Unlike the limitation of the disturbance coefficient of the nonlinear system in H-DOB is constant, in the BR-DCT powertrain system, the disturbance coefficient is expressed as a function of time rather than a constant. Therefore, when H-DOB is used for BR-DCT dis-

turbance estimation, the convergence of error dynamics cannot be guaranteed [26]. Therefore, an extended type of disturbance observer is needed that can guarantee the convergence of H-DOB error dynamics for the case where the disturbance coefficient is time-varying.

Therefore, in this study, an Extended H-DOB (EH-DOB) based on H-DOB is proposed to design a disturbance observer for estimating the clutch actuator uncertainty of BR-DCT. To verify the proposed EH-DOB, the disturbance estimation performance is verified using a powertrain test bench that simulates a vehicle equipped with BR-DCT.

The contribution of this paper is as follows. First, an Extended H-DOB that extends an applicable system based on H-DOB is proposed. The convergence of the proposed EH-DOB is verified through estimation error dynamics. Second, to estimate the actuator uncertainty of BR-DCT, EH-DOB was applied as a disturbance estimator.

Section II deals with the problem definition for estimating the actuator model uncertainty of the BR-DCT. In Section III, an Extended H-DOB is proposed and designed for uncertainty estimation. Section IV performs experimental verification using a powertrain test bench to verify the proposed method. Finally, this work is concluded in Section V.

II. PROBLEM DEFINITION

A. BR-DCT system modeling and design

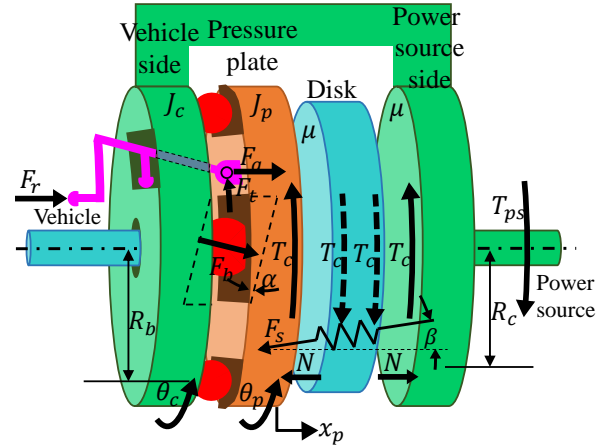


Figure 2. Free-body diagram of BR-DCT.

Referring to the free-body diagram (FBD) of BR-DCT (Fig. 2), The force and torque balance equation can be derived as follows [17], [18].

$$J_p \ddot{\theta}_p = F_t R_a + T_c - F_b R_b \sin \alpha - F_s R_s \sin \beta \quad (1)$$

$$m_p \ddot{x}_p = F_a + F_b \cos \alpha - F_s \cos \beta - N \quad (2)$$

$$F_t = L(\theta_{BR}) F_a \quad (3)$$

$$T_c = \mu N R_c \quad (4)$$

$$x_p = R_b \theta_{BR} \tan \alpha \quad (5)$$

$$\theta_{BR} = \theta_p - \theta_c \quad (6)$$

Table I
DESCRIPTION OF EACH NOTATIONS

Symbol	Name	Symbol	Name
N	Clutch disk Normal force	μ	Clutch disk friction coefficient
a, b	Lever force moment arms	a_f, b_f	Lever friction force moment arms
$L(\theta_{BR})$	Translation to rotation conversion ratio	α	Ramp angle
β	Return spring angle	F_r	Release bearing force
F_a	Clutch actuator force	F_t	Clutch actuator rotational force
F_s	Return spring force	F_b	Ball reaction force
R_a	Lever actuation radius	R_b	Ball actuation radius
R_c	Clutch disk effective radius	R_s	Return spring actuation radius
T_c	Clutch friction torque	T_{ps}	Power source torque
θ_p	Pressure plate rotation angle	θ_c	Vehicle side plate rotation angle
θ_{BR}	Ball-ramp actuation angle	x_p	Pressure plate displacement
J_p	Pressure plate inertia	J_c	Vehicle side plate inertia
m_p	Pressure plate mass	m_c	Vehicle side plate mass

(1), (2) and (3) are the torque, force and lever balance equations, (4) is the clutch friction torque equation and (5), (6) are ball-ramp mechanism constraints, respectively. Here, since the rigidity of the pressure plate and ball is high, it is assumed that their deformation is neglected. Also, it is assumed that N can be obtained using a pre-defined disk compression kinematics and actuator encoder measurement. To derive $L(\theta_{BR})$, lever's FBD can be used as shown in the Fig. 3.

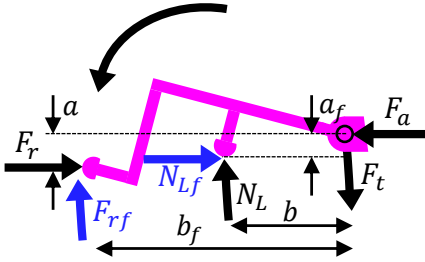


Figure 3. Free-body diagram of self-energizing actuation lever.

As can be seen from the figure, it can be assumed that the inertia term is ignored because the mass of the lever is very small. Therefore, the following equations can be derived.

$$F_a = \left(1 + \mu_L \frac{\mu_L b_f - a}{\mu_L a_f + b}\right) F_r = T_r^a(\theta_{BR}) F_r \quad (7)$$

$$F_t = \frac{\mu_L^2 a_f + a + \mu_L(b - b_f)}{\mu_L^2 b_f + b + \mu_L(a_f - a)} F_a = L(\theta_{BR}) F_a \quad (8)$$

where, F_r is the force exerted by the release bearing on the clutch actuator lever, and N_L is the rotational reaction force generated from the vehicle side plate. In addition, F_{rf} and N_{Lf} are frictional forces generated by F_L and N_L ,

respectively. a, b, a_f and b_f are moment arms of F_r, N_L, N_{Lf} and F_{rf} , respectively. Also, β is the angle of the return spring. This value changes according to θ_{BR} , and it is assumed that it can be obtained using a pre-defined kinematics and actuator encoder. μ_L is the coefficient of friction between the lever and vehicle side plate. Using the (7), F_a can be obtained from the release bearing force (F_r). In addition, $L(\theta_{BR})$ used in (3) can be obtained from (8).

Using the above equations, the clutch torque equation can be derived as follows.

$$T_c = \mu R_c \frac{R_b \tan \alpha + LR_a}{R_b \tan \alpha - \mu R_c} F_a - \mu R_c \frac{R_s \sin \beta + R_b \tan \alpha \cos \beta}{R_b \tan \alpha - \mu R_c} F_s \quad (9)$$

$$G = \frac{R_b \tan \alpha + LR_a}{R_b \tan \alpha - \mu R_c} \quad (10a)$$

$$G_s = \frac{R_s \sin \beta + R_b \tan \alpha \cos \beta}{R_b \tan \alpha - \mu R_c} \quad (10b)$$

In (9), the coefficient of $\mu R_c F_a$ is defined as self-energizing gain (G), and the coefficient of $\mu R_c F_s$ is defined as return spring gain (G_s). BR-DCT can be designed to reduce clutch actuator energy consumption compared to conventional DCT by selecting design parameters to satisfy several constraints for G and G_s [17], [18]. Here, it is assumed that R_a, R_b , and R_c are the constant size parameters of the clutch pack and are determined in advance according to the target size.

If (4) is applied to the left side of (9), equation can be summarized as follows.

$$N = \frac{R_b \tan \alpha + LR_a}{R_b \tan \alpha - \mu R_c} F_a - \frac{R_s \sin \beta + R_b \tan \alpha \cos \beta}{R_b \tan \alpha - \mu R_c} F_s \quad (11)$$

In addition, (11) can be summarized for μ as follows.

$$\mu = \frac{R_b \tan \alpha}{R_c} - \frac{(R_b \tan \alpha + LR_a) F_a}{R_c N} - \frac{(R_s \sin \beta + R_b \tan \alpha \cos \beta) F_s}{R_c N} = f(\theta_{BR}, F_a) \quad (12)$$

In (12), $L(\theta_{BR}), \beta, F_s$ and N are variables determined by θ_{BR} . Therefore, (12) can be expressed as follows.

$$T_c = -F_a \{LR_a + R_b \tan \alpha\} + F_s (R_s \sin \beta + R_b \cos \beta \tan \alpha) + R_b N \tan \alpha = f(\theta_{BR}, F_a) \quad (13)$$

Unlike the actuator model used in the conventional DCT (4), the above equation does not include the friction coefficient μ . As mentioned above, the change in the clutch friction coefficient in DCT is the dominant factor of actuator model uncertainty. That is, BR-DCT can remove μ from the clutch

Table II
SELECTED DESIGN PARAMETERS OF THE BR-DCT

Name	Value
R_a	92.7mm
R_s	119.5mm
R_c	92.7mm
R_b	91mm
α	30°
$\min \beta$	6°
$G(\mu = 0.4)$	9.40
$G_s(\mu = 0.4)$	0.10

Table III
PARAMETERS OF THE TARGET VEHICLE

Name	Value
Mass	1400kg
Max. Power source torque	250Nm

torque equation only by measuring the position and force of the clutch actuator using the improved actuator model of equation (13). By using this method, it is possible to substantially eliminate the degradation of shift control performance caused by actuator model uncertainty in conventional DCT.

The design parameters of BR-DCT are selected as shown in Table II to reduce clutch actuator energy consumption, maintain engagement with negative torque, and reduce reverse torque when tie-up occurs.

The constraints proposed in the previous study [17] can be briefly expressed as follows.

- 1) $\tan \alpha > \mu \frac{R_c}{R_b}$: To prevent self-locking.
- 2) $G > 1, \beta \rightarrow 0$: To reduce the energy consumption of the clutch actuator.
- 3) $\tan \alpha > \mu \frac{R_c(1 + \eta)}{R_b(1 - \eta)}$: To maintain engagement even when negative torque occurs, such as a power source brake. ($\eta = \frac{T_{ps.negative.max}}{T_{ps.max}}$)

The specifications of the target vehicle used in the design of the BR-DCT using the above constraints are as shown in Table III. In addition, for the use of the improved actuator model, a force sensor can be mounted on the actuator output. Through this process, a prototype of BR-DCT was designed and manufactured as shown in Fig. 4.

B. Problem definition

To use the improved actuator modeling of BR-DCT, the position(θ_{BR}) and force(F_a) of the clutch actuator must be measured. Position can be measured with an encoder or Hall sensor equipped for position control of the clutch actuator. The force can be measured using the current and torque constant of the motor, but the measurement accuracy is poor due to the friction of the ball screw of the linear actuator used as a clutch actuator. Therefore, it is possible to install a force sensor inside the dual-clutch pack or output of the linear actuator of BR-DCT. Because BR-DCT's clutch actuator uses the self-energizing principle, clutch torque can be generated

even with a small actuator force. Therefore, as the capacity of the force sensor decreases, the price and size decrease, thus minimizing the additional costs for sensor installation. However, it is difficult to install the force sensor inside the clutch pack because it is connected to the power source and always rotates during shifting. Therefore, a force sensor can be installed at the output of the linear actuator to measure the release bearing force (F_r). (Fig. 5) In this way, the clutch torque can be calculated using F_a and θ_{BR} measured by the sensor of the clutch actuator and the equations (12) and (13). (Fig. 6 (b))

For verification of the improved clutch actuator model of BR-DCT proposed in equation (13), the clutch torque (T_c) can be calculated by inputting the position and force measurements into the actuator inverse model. However, as can be seen in Fig. 6 (b), clutch torque measured by the torque sensor installed for verification and clutch torque calculated using the actuator model of BR-DCT are somewhat different. Referring to the graph showing the error of clutch torque calculation (Fig. 6 (c)), calculation error increases as clutch torque increases. Specifically, the error is small when the magnitude of clutch torque is relatively small, such as during the torque phase, in which the torque exchange between the on-coming clutch and the off-going clutch occurs. However, the error is large when clutch torque is large, such as during the inertia phase that synchronizes the speed of the on-coming clutch and the power source. That is, because error increases as the force of the clutch actuator increases, force and error are proportional. The main cause of this error is the friction of the components between the force sensor and the actual F_a . (Fig. 7) Considering that the friction force is proportional to the normal force, friction between parts is the main factor in the torque calculation error because friction force increases as actuator force increases.

An additional factor is a change in the direction of the lever friction force. The FBD of the lever as can be seen in (Fig. 3) shows the case of rotating counterclockwise. However, when the lever rotates clockwise, the direction of the lever friction, indicated by the blue arrow, is reversed. Therefore, (7) and (8) changes as follows.

$$F_a = \frac{\mu_L(a - a_f) + b + \mu_L^2 b_f}{b - \mu_L a_f} F_r \quad (14)$$

$$\frac{(2 + \mu_L^2)a_f - \mu_L(b - b_f)}{\mu_L^2 b_f + \mu_L a_f + \mu_L a + b} F_a = L_{inv}(\theta_{BR}) F_a = F_t \quad (15)$$

Referring to these equations, the clutch actuator model changes according to the rotation direction of the lever. However, the friction coefficient μ_L between the lever and the plate is relatively small because this is a case of friction between metals. ($\mu_L = 0.05 - 0.1$) Therefore, the magnitude of the error due to the model change of the clutch actuator according to the rotation direction of the lever is also small. However, because it is not negligibly small, it needs to be estimated as model uncertainty, along with the friction of the components.

To solve this problem, in this paper, the uncertainty caused by friction between parts and the change of the lever model is

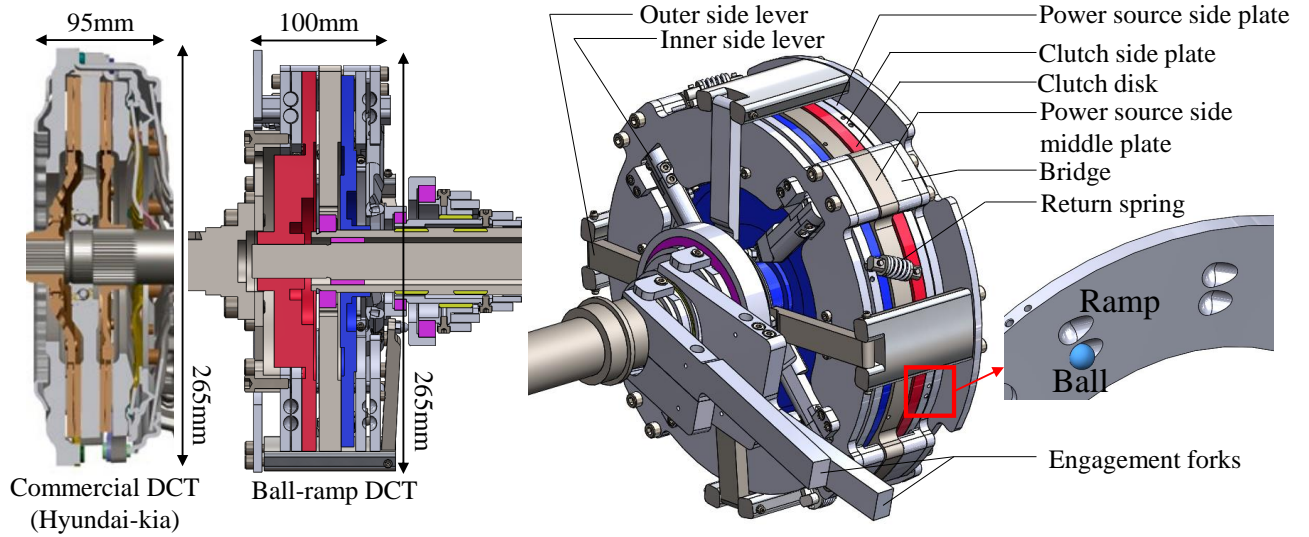


Figure 4. A prototype of BR-DCT. Left: Comparison of cross-section between BR-DCT and commercial DCT (Hyundai-Kia [27]). Right: Names of each part of BR-DCT and ball and ramp structure.

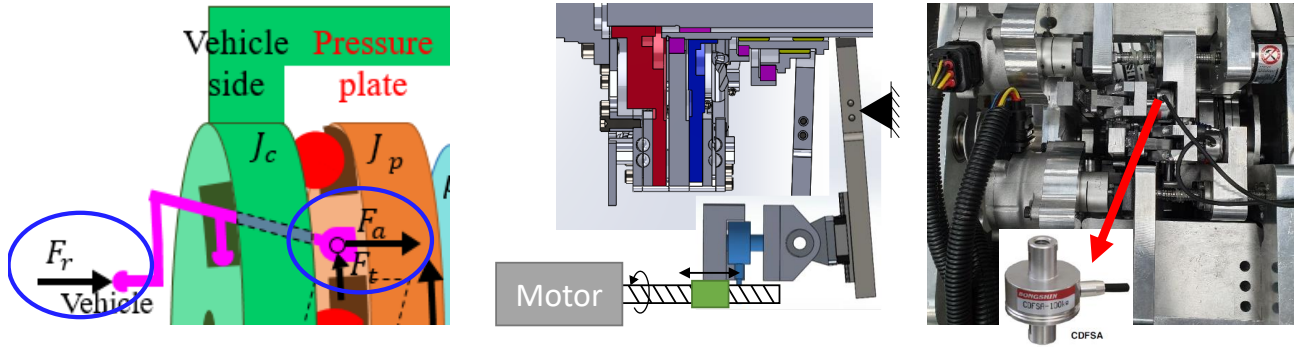


Figure 5. A force sensor was installed to measure F_a . Because the clutch pack is always rotating, the force sensor is installed at the output of the clutch actuator.

estimated. Here, model uncertainty assumes that the measurement error of the force sensor mainly caused by friction of parts is the most dominant, and it is defined as d . Therefore, the unit of d can be set to Newton(N).

For accurate estimation, an estimation method should be selected in consideration of uncertainty and the characteristics of the target system. First, referring to the equation (13), it can be seen that it is a nonlinear system. Also, it is necessary to consider that uncertainty changes with time. (Fig. 1) Therefore, it is inappropriate to use parameter adaptation or a constant disturbance observer suitable for estimating constant uncertainty in a linear system. Therefore, a nonlinear disturbance observer can be used. That is, nonlinear harmonic DOB [23] and high-order DOB (H-DOB) [24] can be used. However, it is necessary to consider that only limited information on disturbance can be used. Therefore, a nonlinear harmonic DOB that requires more information is inappropriate to use. Therefore, in this paper, H-DOB is used to estimate the model uncertainty of the actuator.

However, since the pressure plate mass and inertia were

neglected in the actuator dynamics of BR-DCT expressed in (13), actuator modeling of BR-DCT is not suitable for use in DOB's plant model. Therefore, a target system plant using the powertrain model (Fig. 9) is used together. This method is mainly used for uncertainty estimation of conventional DCT clutch actuators [19]–[21], [28], [29]. As shown in Fig. 9, a DCT-equipped powertrain model can be established. When using this model, the values that can be measured with in-vehicle sensors are the drive torque and speed of the power source, clutches 1/2, and the wheel. In addition, the drive shaft torque is obtained by multiplying the drive shaft torsion angle (measured by the encoder) by the shaft spring constant using a torsion model. When using the powertrain model, an external disturbance called road load torque (T_v) must be considered. In this model, the values that can be measured for disturbance estimation are the power source torque and the drive torque. Therefore, only two uncertainties can be estimated. Here, the uncertainty to be estimated is the force sensor error of the two clutches (d) and the road load torque (T_v). Fortunately, in the torque phase, where two uncertainties have to be estimated,

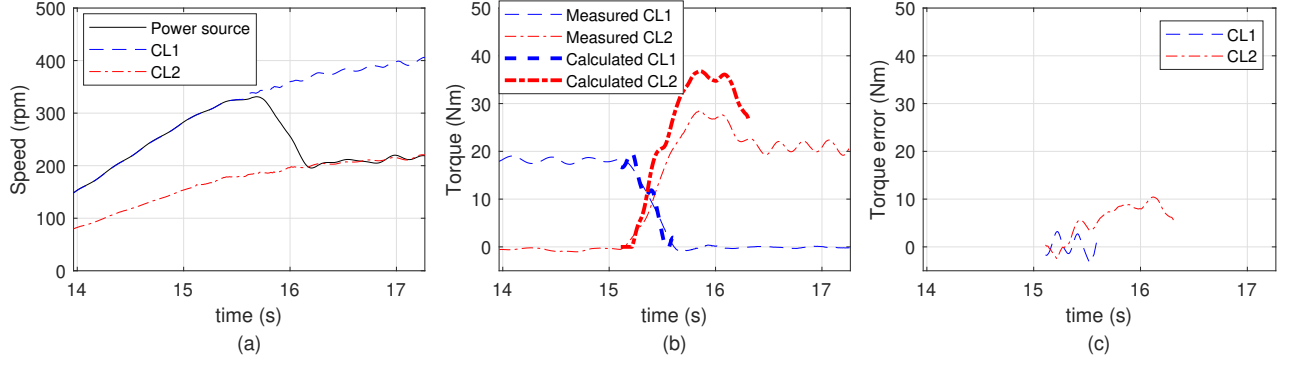


Figure 6. Using the improved actuator model of BR-DCT can reduce model uncertainty, but a small amount of uncertainty occurs due to friction between actuator parts, so the error increases as the clutch torque increases. This phenomenon can be seen as a result of torque calculation using the actuator inverse model during shift control. (CL1: Clutch 1, CL2: Clutch 2)

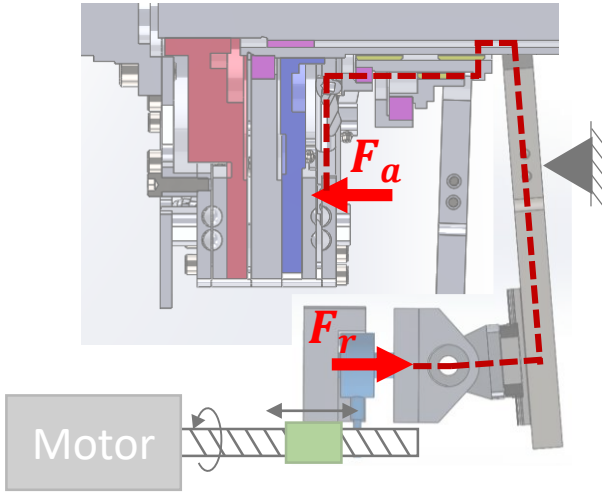


Figure 7. There are many parts between the pressure plate and the force sensor mounted on the actuator output. The bearing friction of these parts creates an error between F_a and the value measured by the force sensor.

the magnitude of the uncertainty is small because the clutch torque is relatively small. Therefore, in the inertia phase where the model error becomes large, a BR-DCT powertrain model can be used for estimation of the actuator model uncertainty (d) and road load torque (T_v) of the oncoming clutch.

The BR-DCT powertrain model for model uncertainty estimation is expressed by the following equations.

$$J_{ps}\dot{\omega}_{ps} = T_{ps} - T_{c1} - T_{c2} \quad (16)$$

$$J_{eq2} \frac{\dot{\omega}_{c2}}{r_2 f r_2} = r_2 f r_2 T_{c2} - T_d \quad (17)$$

$$J_v \dot{\omega}_v = T_d - T_v = k_d(\theta_d - \theta_v) + c_d(\omega_d - \omega_v) - T_v \quad (18)$$

The notation for variables used in these expressions is given in table IV. (13) can also be used to use BR-DCT clutch actuator modeling. Here, L , β , and N are determined by the actuator position (θ_{BR}), so (13) can be expressed as (19).

$$T_{c2} = -(F_a + d)f_1(\theta_{BR}) + f_2(\theta_{BR}) \quad (19)$$

$$f_1(\theta_{BR}) = 2\{LR_a + R_b \tan \alpha\} \quad (20)$$

$$f_2(\theta_{BR}) = 2F_s(R_s \sin \beta + R_b \cos \beta \tan \alpha) + 2R_b N \tan \alpha \quad (21)$$

Table IV
DESCRIPTION OF POWERTRAIN MODEL NOTATIONS

Symbol	Name	Symbol	Name
J_{ps}	Power source inertia	J_{eq2}	Clutch 2 equivalent inertia
J_v	Vehicle inertia	ω_{ps}	Power source rotation speed
ω_{c2}	Clutch 2 rotation speed	ω_v	Wheel rotation speed
ω_d	Drive shaft rotation speed	θ_d	Drive shaft rotation angle
θ_v	Wheel rotation angle	T_{ps}	Power source torque
T_{c1}	Clutch 1 torque	T_{c2}	Clutch 2 torque
T_d	Drive shaft torque	T_v	Road load torque
r_1	First gear ratio	r_2	Second gear ratio
$f r_1$	First final gear ratio	$f r_2$	Second final gear ratio
k_d	Drive shaft stiffness	c_d	Drive shaft compliance

The BR-DCT actuator model of (19) is expressed in the form of a state space with the powertrain model of the equations (16), (17), and (18) as follows. At this time, since IP is assumed, $T_{c1} = 0$.

$$\dot{x} = f(x) + b_u(t)u + b_d(t)D \quad (22a)$$

$$y = Cx \quad (22b)$$

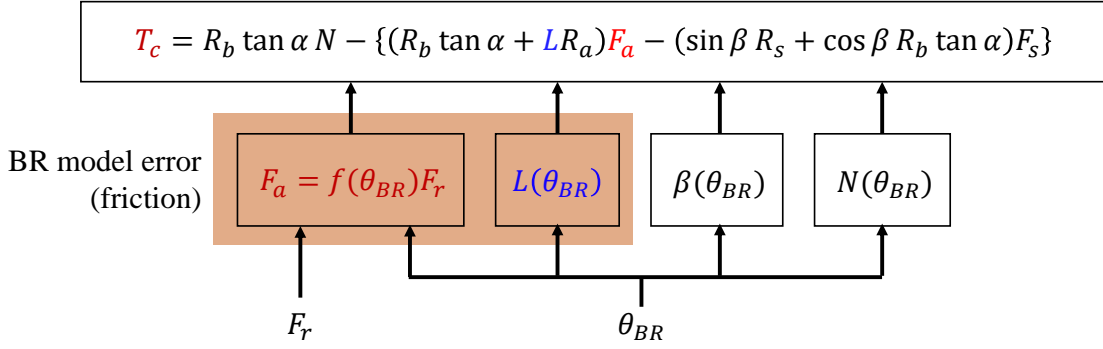


Figure 8. Uncertainties caused by actuator model error of BR-DCT.

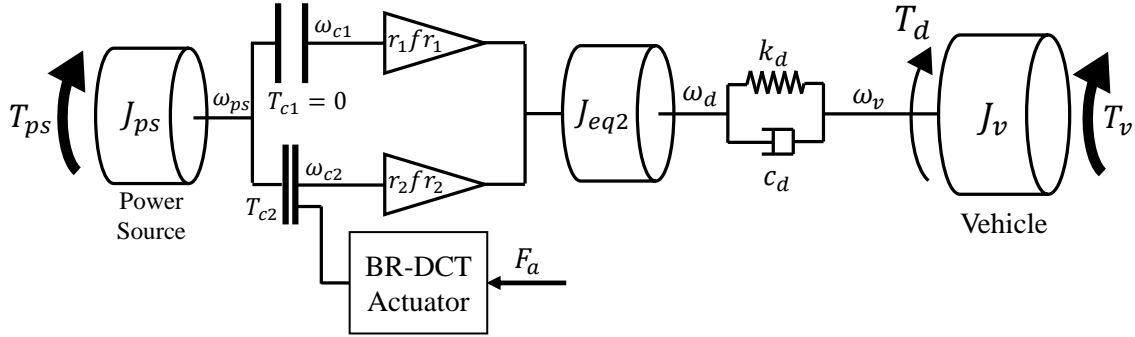


Figure 9. BR-DCT powertrain modeling.

$$\begin{aligned}
 \mathbf{x} &= \begin{bmatrix} \omega_{ps} - \omega_{c2} \\ \omega_{c2} \\ r_2 f r_2 \\ T_d \end{bmatrix}, \\
 \mathbf{f}(\mathbf{x}) &= \begin{bmatrix} -\left(\frac{1}{J_{ps}} + \frac{(r_2 f r_2)^2}{J_{eq2}}\right) f_2(\theta_{BR}) + \frac{r_2 f r_2 T_d}{J_{eq2}} \\ \frac{r_2 f r_2}{J_{eq2}} f_2(\theta_{BR}) - \left(\frac{1}{J_{eq2}} + \frac{1}{J_v}\right) T_d \\ \left\{ \frac{c_d r_2 f r_2}{J_{eq2}} f_2(\theta_{BR}) + k_d \left(\frac{\omega_{c2}}{r_2 f r_2} - \omega_v\right) \right. \\ \left. - c_d \left(\frac{1}{J_{eq2}} + \frac{1}{J_v}\right) T_d \right\} \end{bmatrix}, \\
 \mathbf{b}_u(t) &= \begin{bmatrix} \frac{1}{J_{ps}} \left(\frac{1}{J_{ps}} + \frac{(r_2 f r_2)^2}{J_{eq2}}\right) f_1(\theta_{BR}) \\ 0 \\ 0 \\ 0 \end{bmatrix}, \quad \mathbf{u} = \begin{bmatrix} T_{ps} \\ F_a \end{bmatrix}, \\
 \mathbf{b}_d(t) &= \begin{bmatrix} 0 \\ \frac{1}{J_v} \\ \frac{c_d}{J_v} \\ \frac{1}{J_v} \end{bmatrix}, \\
 \mathbf{D} &= \begin{bmatrix} T_v \\ d \end{bmatrix}, \quad \mathbf{C} = \begin{bmatrix} 1 & 0 & 0 \\ 0 & 1 & 0 \\ 0 & 0 & 1 \end{bmatrix}
 \end{aligned} \tag{23}$$

where x is the system state vector, u is the system input vector, D is the system uncertainty, and y is the system output. However, as expressed in (21) and (22), the disturbance coefficient (b_d) of the target system in the powertrain model is a variable, not a constant. In H-DOB, the disturbance coefficient of the target nonlinear system must be constant so that the error converges to zero. Therefore, the convergence of error dynamics cannot be guaranteed when H-DOB is used for BR-DCT disturbance estimation. Therefore, when the disturbance coefficient is a variable, an extended form of H-DOB that can guarantee the convergence of error dynamics is required.

Therefore, in this study, a new H-DOB-based disturbance estimation method was proposed to design the DOB for BR-DCT uncertainty estimation. In this process, the convergence of error dynamics when H-DOB is applied to a system in which the disturbance coefficient is not constant was investigated. Afterward, an algorithm of Extended H-DOB was proposed to ensure convergence of error dynamics.

III. PROPOSED THE EXTENDED HIGH-ORDER DISTURBANCE OBSERVER

A. Limitations of High-order Disturbance Observer

As mentioned in the chapter I, H-DOB has limitations on the applicable nonlinear system structure. In particular, the disturbance coefficient must be constant to ensure convergence of estimation error. Therefore, convergence in a system with a non-constant disturbance coefficient is not guaranteed. In this

subsection, the convergence of the disturbance error when H-DOB is applied to a system with the non-constant disturbance coefficient is verified. Specifically, the convergence when using H-DOB in the applicable system is compared with the disturbance coefficient is not constant.

First, the nonlinear system that guarantees the convergence of H-DOB error dynamics can be expressed as follows.

$$\dot{x} = f(x, u; t) + Fd \quad (24)$$

where, it is assumed that $x \in \mathbb{R}^n, u \in \mathbb{R}^m, d \in \mathbb{R}^r, f(\cdot)$ and the coefficient of disturbance F which is $\text{rank}(F) = r$ are known. Here, $f(x, u; t)$ is a smooth function with time. Multiplying both sides of (24) by F^+ , which is the Moore-Penrose pseudo-inverse of the disturbance coefficient F , as follows.

$$F^+ \dot{x} = F^+ f(x, u; t) + d \quad (25)$$

The given disturbance information is as follows.

$$d(t) = \sum_{k=0}^q d_i t^k \quad (26)$$

where $d_i, (i \in \{0, \dots, q\})$ is a constant, but unknown.

To estimate d in a nonlinear system (24), the following DOB can be designed.

Theorem 1 (H-DOB). *Given matrices $\Gamma_k = \text{diag}\{\gamma_{k1}, \dots, \gamma_{kr}\}$ and $(k \in \{0, \dots, q\})$, suppose that γ_{ij} s are chosen such that the polynomials $p_j(s)$ are Hurwitz stable, where*

$$p_j(s) = s^{q+1} + \gamma_{0j}s^q + \gamma_{1j}s^{q-1} + \dots + \gamma_{(q-1)j}s + \gamma_{qj} \quad (27)$$

for $j = 1, \dots, r$. Then disturbance estimate given by

$$\hat{d}(t) = \sum_{k=0}^q \Gamma_k g_k(t) \quad (28)$$

is asymptotically convergent to the high-order disturbance, where, $g_k(t)$ s are defined by

$$g_k(t) = \begin{cases} F^+ x - z & (k=0) \\ \int_0^t g_{k-1} d\tau & (k \geq 1) \end{cases} \quad (29)$$

where the internal state of the DOB z is defined by

$$\dot{z} = F^+ f(x, u; t) + \hat{d} \quad (30)$$

Proof. To investigate the convergence of H-DOB error dynamics, an estimation error expressed as $e_d = \hat{d} - d$ can be introduced. At this time, the derivative of e_d is as follows.

$$\dot{e}_d = \dot{\hat{d}} - \dot{d} = \dot{\hat{d}} - \Gamma_0 \dot{g}_0(t) - \dots - \Gamma_q \dot{g}_q(t) \quad (31)$$

Using $\dot{g}_k(t) = \begin{cases} e_d, & (k=0) \\ g_{k-1}(t), & (k \geq 1) \end{cases}$, the (31) is expressed as

$$\dot{e}_d = \dot{\hat{d}} - \Gamma_0 e_d - \Gamma_1 g_0(t) - \dots - \Gamma_q g_{q-1}(t) \quad (32)$$

The result of the $(q+1)$ -th derivative of e_d in (32) is as follows.

$$e_d^{(q+1)} + \Gamma_0 e_d^{(q)} + \dots + \Gamma_q e_d = d^{(q+1)} \quad (33)$$

Here, $(\cdot)^{(k)}$ means the k -th derivative of the function. According to the disturbance information in the (26), $d^{(q+1)} = 0$. Therefore, the j -th row of the Laplace transform of (33) is expressed as follows.

$$E_{dj}(s)(s^{q+1} + \gamma_{0j}s^q + \dots + \gamma_{(q-1)j}s + \gamma_{qj}) = 0 \quad (34)$$

The characteristic equation of error dynamics can be obtained through (34). Since all the poles of the characteristic equation are in the LHP by *Theorem 1*, the error dynamics of H-DOB are asymptotically and exponentially stable to the initial error. \square

However, in this paper, the coefficient of disturbance (F) is a variable in (22), which is the target system of DOB. This system can be expressed as

$$\dot{x} = f(x, u; t) + F(t)d \quad (35)$$

$$F^+(t)\dot{x} = F^+(t)f(x, u; t) + d \quad (36)$$

Here, $F(t)$ is the component-wise differentiation along the time. That is, $F(t)$ be a matrix of elements $f_{ij}(t)$ which are differentiable functions of time. Also, since the pseudo-inverse of $F(t)$ is unique, (36) obtained by multiplying both sides of (35) by $F^+(t)$ is unique.

To investigate the convergence of error dynamics of H-DOB applied to this system, (32) is rewritten as follows.

$$\dot{e}_d = \Gamma_0 \dot{F}^+(t)x - \Gamma_0 e_d + \Gamma_1 g_0(t) + \dots + \Gamma_q g_{q-1}(t) - \dot{d} \quad (37)$$

The $(q+1)$ -th derivative of (37) is as follows.

$$e_d^{(q+1)} + \Gamma_0 e_d^{(q)} + \dots + \Gamma_q e_d = \Gamma_0 \{F^+(t)x\}^{(q)} + \Gamma_1 \{F^+(t)x\}^{(q-1)} + \dots + \Gamma_q F^+(t)x + d^{(q+1)} \quad (38)$$

As can be seen from the $(q+1)$ -th derivative of (38) with respect to e_d , the characteristic equation of error dynamics such as (34) is not derived because the differential term of $\dot{F}^+(t)x$ remains. Therefore, the convergence of error dynamics cannot be guaranteed.

As such, the convergence of H-DOB cannot be guaranteed in the system expressed by $F(t)$. Here, the system expressed by $F(t)$ can represent the nonlinearity of the input system because F is a function multiplied by u . Therefore, although infrequently, various systems satisfy this condition. In a mechanical system, the function F may have a characteristic that changes with time mainly from the mechanism of the actuator. A typical example is a system in which F changes due to deformation of the lever or a change in clutch friction coefficient while the force generated from the actuator is transmitted to the clutch through the lever mechanism, such as BR-DCT. As such, a system that has a mechanism in the input

actuator, or a system that changes according to temperature or the surrounding environment, causes a change in F with time. In such a system, another method for estimating the disturbance expressed in a polynomial is required.

B. Extended High-order disturbance observer

In order to compensate for the fact that the convergence of H-DOB error dynamics is not guaranteed in a nonlinear system with a non-constant disturbance coefficient, the Extended High-order Disturbance Observer (EH-DOB) proposed in this paper is as follows.

Theorem 2 (EH-DOB). *Given matrices $\Gamma_k = \text{diag}\{\gamma_{k1}, \dots, \gamma_{kr}\}$ and $(k \in \{0, \dots, q\})$, suppose that γ_{ij} 's are chosen such that the polynomials $p_j(s)$ are Hurwitz stable for $j = 1, \dots, r$. Then, the disturbance estimate given by*

$$\begin{cases} \dot{z} = \dot{F}^+(t)x + F^+f(t) + \hat{d} & (39a) \\ \hat{d} = \sum_{k=0}^q \Gamma_k g_k(t) & (39b) \end{cases}$$

is asymptotically convergent to the high-order disturbance d , where $g_k(t)$'s are defined by

$$g_k(t) = \begin{cases} F^+(t)x - z, & (k = 0) \\ \int_0^t g_{k-1} d\tau, & (k \geq 1) \end{cases} \quad (40)$$

Proof. To investigate the convergence of the error dynamics of the proposed EH-DOB, e_d can be rewritten as follows using (39).

$$e_d = \dot{F}^+(t)x + F^+(t)\dot{x} - \dot{z} \quad (41)$$

The derivative of the above expression is as follows.

$$\begin{aligned} \dot{e}_d = \dot{d} - \dot{\hat{d}} = \dot{d} - \Gamma_0(\dot{F}^+(t)x + F^+(t)\dot{x} - \dot{z}) - \Gamma_1 g_0(t) \\ - \dots - \Gamma_q g_{q-1}(t) \end{aligned} \quad (42)$$

$$\dot{e}_d = \dot{d} - \Gamma_0 e_d - \Gamma_1 g_0(t) - \dots - \Gamma_q g_{q-1}(t) \quad (43)$$

The $(q+1)$ -th derivative of (43) is as follows.

$$e_d^{(q+1)} + \Gamma_0 e_d^{(q)} + \dots + \Gamma_q e_d = d^{(q+1)} \quad (44)$$

That is, in (38), the same result is obtained as if there is no derivative term of $\dot{F}^+(t)x$. Therefore, the characteristic equation of error dynamics is derived the same as (34) like H-DOB. Therefore, the error dynamics of EH-DOB are asymptotically and exponentially stable to the initial error. \square

Fig. 10 shows the structure of the proposed Extended High-order Disturbance Observer (EH-DOB). According to the given disturbance information, q can be determined, and $q+1$ Γ 's are designed from the poles of the characteristic equation. If the given disturbance information and the order of EH-DOB are different, steady-state error or oscillation occurs in

Table V
 $e_d(s)$ ACCORDING TO THE VALUE OF q

Case	$e_d(s)$
$q < p$	$\frac{d_0 s^p + d_1 s^{p-1} + \dots + p! d_p}{s^{p-q}(s^{q+1} + \Gamma_0 s^q + \dots + \Gamma_q)}$
$q = p$	$\frac{d_0 s^p + d_1 s^{p-1} + \dots + p! d_p}{s^{q+1} + \Gamma_0 s^q + \dots + \Gamma_q}$
$q > p$	$\frac{(d_0 s^p + d_1 s^{p-1} + \dots + p! d_p) s^{q-p}}{s^{q+1} + \Gamma_0 s^q + \dots + \Gamma_q}$

the convergence of the error. This phenomenon can also be expressed mathematically. For ease of understanding, a system with $r = 1$ is assumed.

First, to summarize (39) for \hat{d} , it is as follows.

$$\hat{d} = \Gamma_0 \dot{g}_0(t) + \Gamma_1 g_0(t) + \dots + \Gamma_q g_{q-1}(t) \quad (45a)$$

$$= \Gamma_0(\dot{F}^+(t)x + F^+(t)x - \dot{z}) + \Gamma_1 g_0(t) + \dots + \Gamma_q g_{q-1}(t) \quad (45b)$$

$$= \Gamma_0 e_d + \Gamma_1 \int e_d + \Gamma_2 \iint e_d + \dots + \Gamma_q \int \dots \int e_d \quad (45c)$$

Here, q is the expected degree of disturbance used in the design of the EH-DOB, and $\int \dots \int_q$ represents the multiple integrations of q times. Also, p is the actual degree of disturbance. The Laplace transform of (45) is as follows.

$$s^{q+1} \hat{d}(s) = (\Gamma_q + \Gamma_{q-1} s + \dots + \Gamma_0 s^q) e_d(s) \quad (46)$$

Summarizing the above expression for $e_d(s) = \hat{d}(s) - d(s)$, it is as follows.

$$e_d(s) = \frac{s^{q+1}}{s^{q+1} + \Gamma_0 s^q + \dots + \Gamma_q} d(s) \quad (47)$$

The disturbance information of (26) is expressed as Laplace transform as follows.

$$d(s) = \frac{d_0 s^p + d_1 s^{p-1} + \dots + p! d_p}{s^{p+1}} \quad (48)$$

By combining (48) and (47), the change in $e_d(s)$ according to the value of q can be obtained. Table V shows $e_d(s)$ where q is less than, equal to or greater than p . Referring to this table, if q is less than p , a pole with a value of 0 is generated, and if it is greater than p , a zero with a value of 0 is generated. That is, if the expected order (q) of the EH-DOB is lower than the actual (p), convergence may decrease, and if it is high, the oscillation may increase. This phenomenon can be seen in the Fig. 11.

Referring the Fig. 11 (a), e_d that changes according to the value of q is showed. If q is greater than p , the oscillation of e_d increases. This can be seen from the analysis of the frequency composition of e_d shown in Fig. 11 (b). Referring to the frequency composition analysis of e_d , it can be seen that the high-frequency component relatively increases as q increases. These oscillations can cause divergence when matched to the

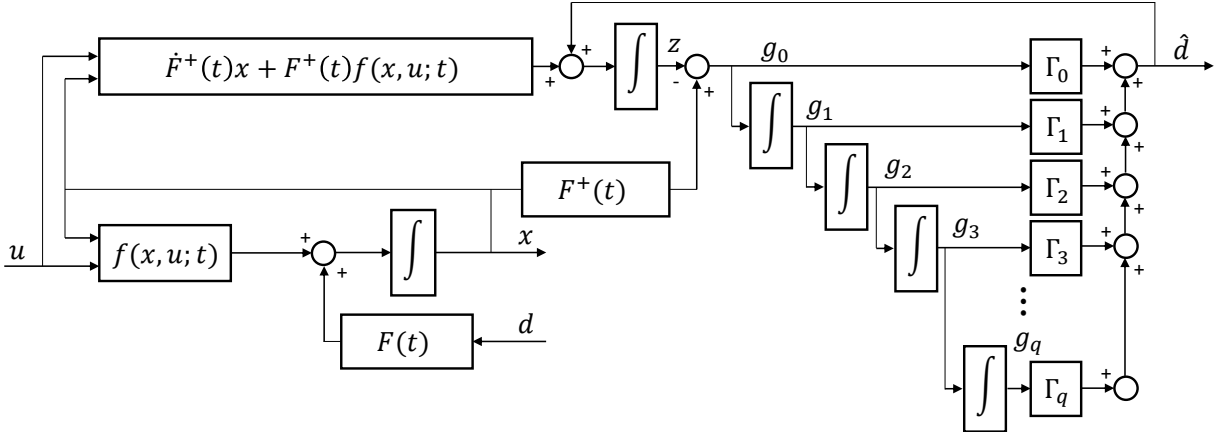


Figure 10. Block diagram of extended high-order disturbance observer (EH-DOB).

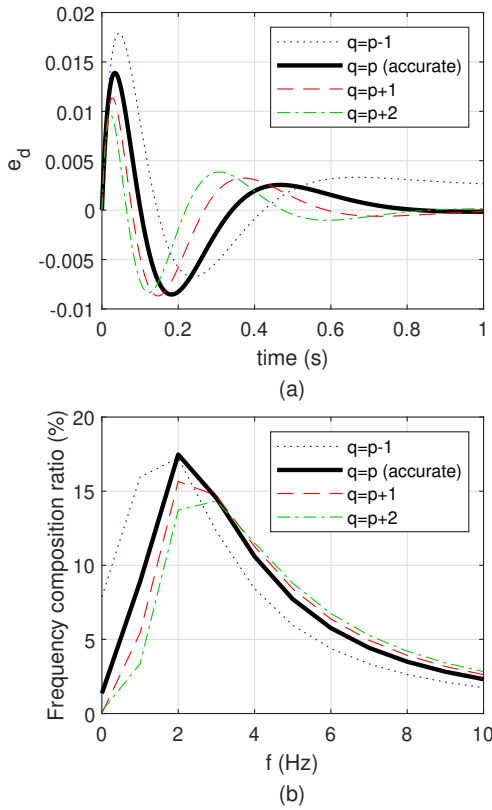


Figure 11. Error fluctuations caused by the difference between the order of EH-DOB (q) and the order of disturbance (q).

resonant frequency of the system. Therefore, when choosing the order of the EH-DOB, q should be selected so that the dominant frequency of e_d avoids the resonant frequency of the system.

As such, the EH-DOB proposed in this paper compensates for the shortcomings of the previous study (H-DOB) and can estimate disturbance in a system with a time-varying coefficient of disturbance, such as BR-DCT. That is, EH-DOB made it possible to apply to various systems by further generalizing the system to which H-DOB is applicable. However, as previ-

ously assumed, the system state x should be measurable, and the order of the expected polynomial disturbance should be chosen to avoid the system's resonant frequency.

Remark 1. If $F(t)$ and d are lumped together and regarded as a new disturbance and expressed as $\Delta = F(t)d$, $F(t)$ of the expanded system is 1, and the disturbance that changes with time is Δ . Therefore, this method has the same effect as increasing the degree of d to Δ . However, since q , which is still the order of disturbance, is set to d , the estimation accuracy is lowered. As a result, the estimation accuracy decreases because the information $F(t)$ provided by the system is not used. Additionally, as mentioned in [24], since the order of Δ is larger than that of d , the estimation performance may be reduced if Δ is not sufficiently slower than the bandwidth of the H-DOB. Furthermore, if (38) is expressed using $\Delta = F(t)d$, there is still a derivative term of $\dot{F}^+(t)x$ left.

C. Design of Disturbance Observer for Actuator Model Uncertainty Estimation

To estimate the uncertainty of the BR-DCT system using the EH-DOB proposed in this paper, the generalization of the BR-DCT powertrain system using (22) is as follows.

$$\dot{x} = f_{BR}(x, u; t) + F_{BR}(t)D \quad (49)$$

$$f_{BR}(x, u; t) = \mathbf{f}(x) + \mathbf{b}_u(t)u \quad (50a)$$

$$F_{BR}(t) = \mathbf{b}_d(t) \quad (50b)$$

Here, $x = \begin{bmatrix} \omega_{ps} - \omega_{c2} \\ \frac{\omega_{c2}}{r_2 f r_2} - \omega_v \\ T_d \end{bmatrix}$ is the state vector of the system,

all of which are measurable, and $D = \begin{bmatrix} d \\ T_v \end{bmatrix}$ is the uncertainty of the BR-DCT powertrain system.

Theorem 2 can be applied to design the EH-DOB of this system. (39) and (40) can be expressed as follows using (49).

Table VI
DESCRIPTION OF POWERTRAIN PARAMETERS

Symbol	Name
J_{ps}	$0.22kg \cdot m^2$
J_{eq2}	$17.65kg \cdot m^2$
r_1	3.85
r_2	2
fr_1	4
fr_2	4.17

$$\begin{cases} \dot{z} = \hat{F}_{BR}^+(t)x + F_{BR}^+(t)f_{BR}(x, u; t) + \hat{D} & (51a) \\ \hat{D} = \sum_{k=0}^q \Gamma_k g_k(t) & (51b) \end{cases}$$

$$g_k(t) = \begin{cases} F_{BR}^+(t)x - z, & (k = 0) \\ \int_0^t g_{k-1} d\tau, & (k \geq 1) \end{cases} \quad (52)$$

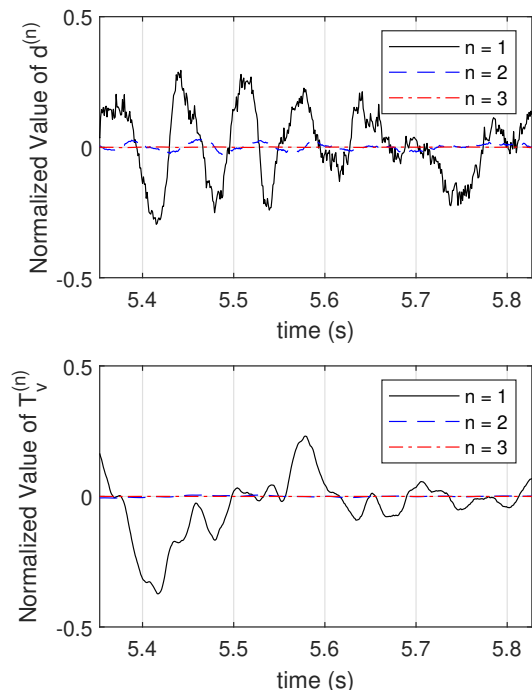


Figure 12. Normalized values of $d^{(n)}$ and $T_v^{(n)}$.

The EH-DOB of the BR-DCT designed by the proposed method used the powertrain parameters in Table VI. In addition, the maximum order of disturbance and the position of each pole in Table VII were specified through actual disturbance analysis. Fig. 12 indicates the normalized value when the disturbance is differentiated. As can be seen in this figure, considering that the third derivative value converges to 0, n and q are selected as 3.

Remark 2. When designing the EH-DOB of BR-DCT using Theorem 2, $f(x, u; t)$ and $F(x, u; t)$ were obtained using the plant of the BR-DCT powertrain. However, it is necessary to consider the role of the DOB when performing disturbance rejection control. When the DOB acts as a controller for

Table VII
DESCRIPTION OF EH-DOB PARAMETERS

Symbol	Name
$n(d^{(n)} = 0)$	3
q	3
$p1$	-10
$p2$	-10
$p2$	-10

disturbance compensation in the form of an inner loop, it can act as a controller to follow the designed model. In this case, the plant used in the DOB design is not necessarily the same as the actual plant. This means that if the real plant has unstable poles, or if the poles are close to the real axis and can cause divergence or oscillation, then the plant used in the DOB can be modified to a stable system [30]. However, the actual value of the disturbance is not known precisely because the difference between the plant used in the DOB and the actual plant is a disturbance to estimate. This issue can be further accentuated in the BR-DCT powertrain. The BR-DCT powertrain model of (22) has a pole of 0 because x_1 is not included on the right side in the dynamics of $x_1 = \omega_{ps} - \omega_{c2}$. To move this unstable pole to the LHP, it is necessary to estimate the disturbance including the state, so the size of the disturbance compensation input increases. Considering that the size of the maximum input is limited due to the limitation of the actuator, if the size of the compensation input is increased, the size of the feedback control input is limited and the control performance may have deteriorated. It also has the potential to diverge if the compensation input exceeds the actuator's bandwidth. In conclusion, in the EH-DOB design for shift control of BR-DCT, disturbance rejection control should be performed using actual plant information.

In summary, like H-DOB, the EH-DOB proposed in this paper is suitable for estimating the disturbance that can be expressed as a polynomial in a system such as (35). In addition, convergence can be guaranteed even in a system with a wider range than H-DOB, such as a system with a non-constant disturbance coefficient. In addition, the method of selecting the order of the polynomial (q) suggested in this paper can prevent error fluctuations and make system resonance. However, since the observer's order must be increased to use the polynomial model, other methods may be more suitable in a system where disturbance is not suitable for polynomial representation.

IV. EXPERIMENTAL VERIFICATION OF PROPOSED ACTUATOR MODEL UNCERTAINTY ESTIMATOR

A. Experimental Setup

A powertrain test bench was constructed to verify the EH-DOB for estimating the actuator model uncertainty of BR-DCT. The test bench was designed to simulate the powertrain of a vehicle equipped with BR-DCT and constructed as a module type.

The test bench consists of a power source, DCT, vehicle, and load module. (Fig. 13) Each module on the test bench is designed to be disassembled or assembled using interchangeable parts. Thus, it is possible to change the target

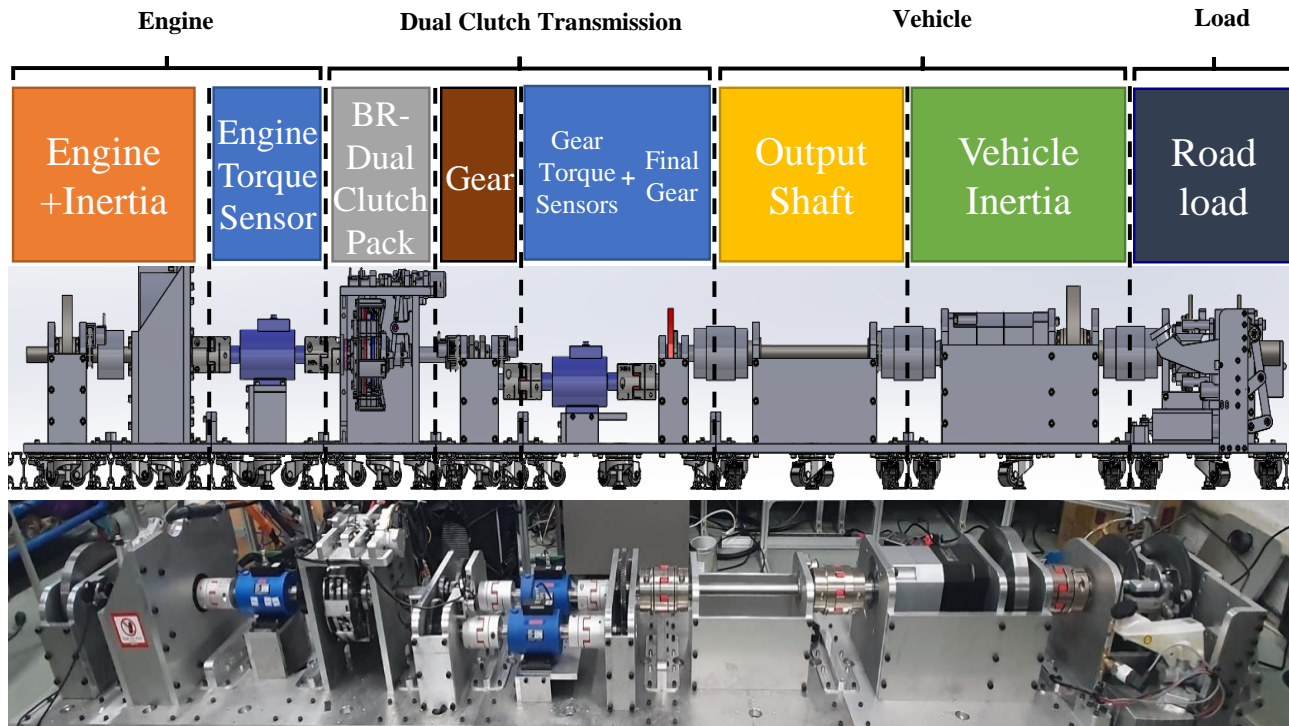


Figure 13. Test bench that simulates the powertrain of a vehicle equipped with BR-DCT. It is equipped with a torque sensor that can measure the torque of the power source and clutches. Each part is designed as a module type and can be replaced.

vehicle or replace the transmission or power source. The power source module uses a Permanent Magnet Synchronous Motor (PMSM) that can output torque of up to $170Nm$. Because this motor has a smaller rotational resistance than that of an engine or electric vehicle drive motor, a disk is connected to model the rotational inertia. The BR-DCT module, which is connected after the power source module, consists of a clutch pack and actuators, gears, torque sensors for verification, and final gears. DCT module is fixed in 1^{st} and 2^{nd} gear to each clutch for installation of torque sensors.

The BR-DCT module used a linear actuator composed of a brushless DC motor (BLDC) and a ball screw as a clutch actuator. It is equipped with an incremental encoder to measure the position and speed of the clutch actuator, and a force sensor to measure the force of the clutch actuator.

The vehicle module is composed of a shaft for modeling oscillation of the drive shaft, a disk plate, and reduction gear for modeling the body mass. The vehicle module used in the test bench is designed to model $1500kg$, which is the weight of a typical passenger car. The load module is designed to generate load torque using an electro-hydraulic brake system.

In the test bench, sensors to verify the proposed method are included. First, an incremental encoder to measure the rotational speeds of the power source, clutches 1 and 2, and the drive shaft is installed. For verification of the proposed algorithm, a rotational torque sensor is mounted on the output of the power source and the shafts of clutches 1 and 2 to measure the power source and clutch torque. In addition, it is possible to control the brake pressure through the hydraulic pressure sensor of the load module. The power source motor,

clutch actuator motor and brake motor are all operated by their respective low-level controllers. These measurement and control systems were constructed using dSpace's MicroAutobox 2 considering applicability to actual vehicles.

B. Verification Experiment Results

To verify the actuator model uncertainty estimation algorithm using the proposed EH-DOB, a shifting scenario corresponding to the inertia phase was selected. In the verification experiment, to compare the proposed method (EH-DOB) with the conventional method (H-DOB), the uncertainty estimation results using H-DOB were also presented. At this time, the order and pole of the H-DOB were selected to be the same as those of the EH-DOB. As mentioned above, H-DOB is a kind of harmonic DOB. However, due to the polynomial expression method of disturbance and the structure targeting nonlinear systems, it has the advantage of being readily applicable to most systems and is easy to tune. EH-DOB is also a kind of harmonic DOB and inherits the advantages of H-DOB. However, it can be viewed as a generalized H-DOB because the applicable system is further expanded. Therefore, it is appropriate to compare the improved stability and performance of EH-DOB compared to H-DOB.

To verify the performance of EH-DOB when shifting, an experimental scenario of shifting from 1^{st} to 2^{nd} gear was used. The results of this verification experiment are shown in Fig. 14.

The experiment begins with the first gear engaged, accelerating while maintaining the power source torque at $16Nm$.

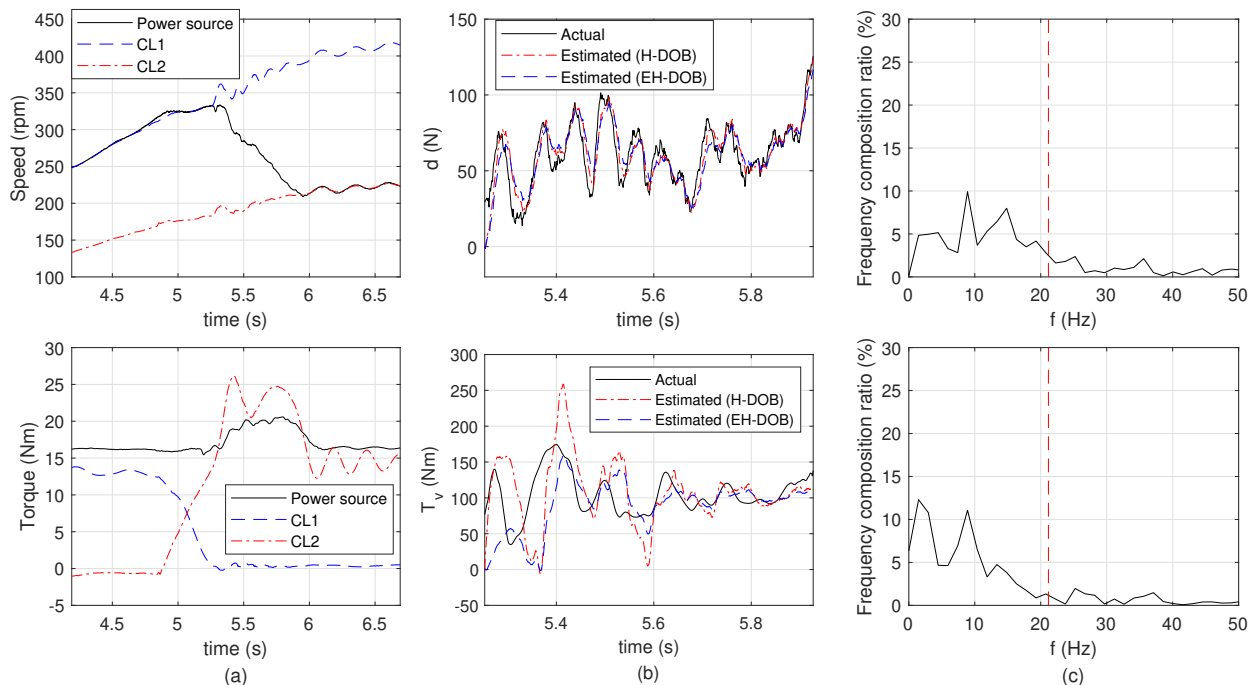


Figure 14. Clutch actuator uncertainty estimation result of BR-DCT using the proposed EH-DOB using shift experiment. (CL1: Clutch 1, CL2: Clutch 2)

When the speed of clutch 1 reaches $300rpm$, the shift controller that receives the shift command performs TP control for about 0.5 seconds and IP control for about 0.8 seconds. As shown in Fig. 14 (a), TP starts at 4.7 seconds and IP starts at 5.3 seconds. As mentioned in chapter II, EH-DOB and H-DOB for estimating actuator uncertainty of BR-DCT can be estimated only from IP. Therefore, from the experimental results in Fig. 14 (b), the uncertainty can be estimated from 5.3 seconds at the start of the IP. Referring to the graph showing the estimation result, the estimated value of the actuator uncertainty by using the EH-DOB (d) shows a slightly high-accuracy estimation performance. Analyzing the cause, since H-DOB assumes F as a constant, the difference becomes larger when F is a time-varying function. Therefore, the convergence of the error dynamics is not guaranteed or the estimation accuracy is lowered despite having the same pole. However, in actuator uncertainty, since the magnitude of the change in F is relatively small, the estimation performance difference may not be large. However, the reason why the error is larger in T_v is that the change in F can act as an input model error of the powertrain and can be regarded as larger model uncertainty. Also, to check whether the dominant frequencies of the estimation errors of d and T_v do not reach the natural frequency of the plant, the frequency composition analysis result of the estimation error is shown in Fig. 14 (c). As a result of the analysis, the dominant frequency of the estimation error was measured to be about 1.5 to 8.9Hz, which is smaller than the natural frequency of the plant at 21.1Hz. (red dotted line)

To verify the repeatability of the proposed method, the same experiment as the above scenario was repeatedly performed. Referring to (Fig. 15), it can be seen that most of the shift

experiment results show high estimation accuracy. Also, in all cases, the dominant frequency of the estimation error was measured to be lower than the resonance frequency of the system. The RMS value of the average estimation error is $11.32N$ for d and $40.04Nm$ for T_v . In conclusion, the uncertainty of the clutch actuator model and the powertrain model estimated through EH-DOB has high accuracy and does not cause plant resonance.

V. CONCLUSION AND FUTURE WORK

In this study, an extended nonlinear disturbance observer was proposed to estimate the uncertainty of the BR-DCT powertrain system. A high-order nonlinear disturbance observer can be used by referring to the results of analyzing the nonlinearity and disturbances in the target system. However, the convergence of the H-DOB error is not guaranteed in a system with a non-constant disturbance coefficient. Therefore, in this paper, an extended high-order disturbance observer was proposed with which the estimation error can converge to zero in a system with a non-constant disturbance coefficient. The proposed EH-DOB can be used to estimate the uncertainty of the clutch actuator model and powertrain model of BR-DCT by extending the system applicable to H-DOB.

The uncertainty of the BR-DCT powertrain system was estimated by applying the proposed EH-DOB, and the pole position of the characteristic equation was also selected considering the maximum disturbance order and the convergence of the error dynamics. To verify the performance of the EH-DOB designed in this method, a shift experiment was performed using the BR-DCT powertrain test bench. As a result, it was verified that the RMS errors of d and T_v were

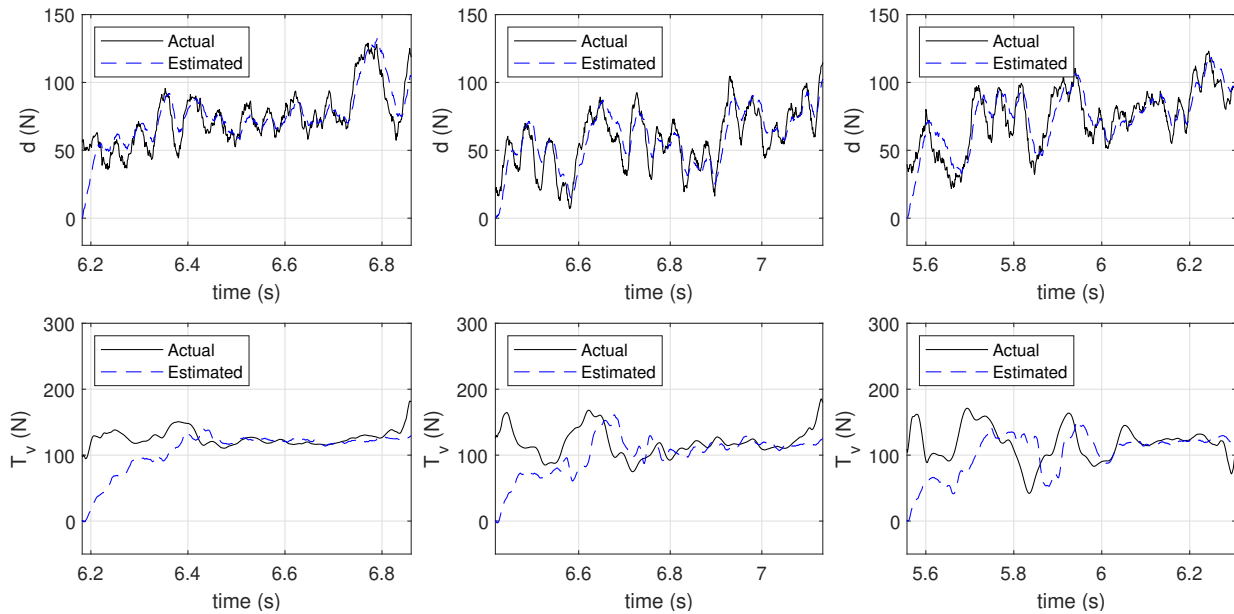


Figure 15. Repeated clutch actuator uncertainty estimation result of BR-DCT using the proposed EH-DOB using shift experiment.

11.32N and 40.04Nm, respectively, showing high estimation accuracy.

For disturbance rejection control using EH-DOB proposed in this paper and feedback controller, it is necessary to design a composite control law that combines the controller input and the disturbance compensation input. At this time, the composite control law should be designed to ensure the stability of the estimation error of the DOB and the tracking error of the controller. These will be dealt with in future work.

ACKNOWLEDGMENTS

This work was supported by the National Research Foundation of Korea(NRF) grant funded by the Korea government(MSIP) (No. 2020R1A2B5B01001531), the Technology Innovation Program (20014983, Development of autonomous chassis platform for a modular vehicle) funded By the Ministry of Trade, Industry Energy(MOTIE, Korea), and the BK21+ program through the NRF funded by the Ministry of Education of Korea.

REFERENCES

- [1] A. Irimescu, L. Mignon, and G. Pădure, "Automotive transmission efficiency measurement using a chassis dynamometer," *International Journal of Automotive Technology*, vol. 12, no. 4, pp. 555–559, 2011.
- [2] A. Turner, K. Ramsay, R. Clark, and D. Howe, "Direct-drive rotary-linear electromechanical actuation system for control of gearshifts in automated transmissions," in *2007 IEEE Vehicle Power and Propulsion Conference*. IEEE, 2007, pp. 267–272.
- [3] H. Kuroiwa, N. Ozaki, T. Okada, and M. Yamasaki, "Next-generation fuel-efficient automated manual transmission," *Hitachi Review*, vol. 53, no. 4, pp. 205–209, 2004.
- [4] M. Kulkarni, T. Shim, and Y. Zhang, "Shift dynamics and control of dual-clutch transmissions," *Mechanism and Machine Theory*, vol. 42, no. 2, pp. 168–182, 2007.
- [5] M. Schuster, "Utilizing an energy-in-energy-out approach to simplify heavy-duty transmission efficiency testing," SAE Technical Paper, Tech. Rep., 2000.
- [6] J. Franco, M. A. Franchek, and K. Grigoriadis, "Real-time brake torque estimation for internal combustion engines," *Mechanical Systems and Signal Processing*, vol. 22, no. 2, pp. 338–361, 2008.
- [7] G. Lucente, M. Montanari, and C. Rossi, "Modelling of an automated manual transmission system," *Mechatronics*, vol. 17, no. 2-3, pp. 73–91, 2007.
- [8] M. Kulkarni, T. Shim, and Y. Zhang, "Shift dynamics and control of dual-clutch transmissions," *Mechanism and machine theory*, vol. 42, no. 2, pp. 168–182, 2007.
- [9] S. Bai, R. L. Moses, T. Schanz, and M. J. Gorman, "Development of a new clutch-to-clutch shift control technology," *SAE Transactions*, pp. 1663–1672, 2002.
- [10] B. Matthes, "Dual clutch transmissions—lessons learned and future potential," *SAE transactions*, pp. 941–952, 2005.
- [11] B. Mashadi, A. Kazemkhani, and R. B. Lakeh, "An automatic gear-shifting strategy for manual transmissions," *Proceedings of the Institution of Mechanical Engineers, Part I: Journal of Systems and Control Engineering*, vol. 221, no. 5, pp. 757–768, 2007.
- [12] C. H. F. Amendola and M. A. L. Alves, "Gear shift strategies analysis of the automatic transmission in comparison with the double clutch transmission," SAE Technical Paper, Tech. Rep., 2006.
- [13] H. Chen and B. Gao, *Nonlinear estimation and control of automotive drivetrains*. Springer Science & Business Media, 2013.
- [14] U. Wagner and A. Wagner, "Electrical shift gearbox (esg)-consistent development of the dual clutch transmission to a mild hybrid system," SAE Technical Paper, Tech. Rep., 2005.
- [15] J. Kim and S. B. Choi, "Design and modeling of a clutch actuator system with self-energizing mechanism," *IEEE/ASME Transactions on Mechatronics*, vol. 16, no. 5, pp. 953–966, 2010.
- [16] J. J. Oh, J. Kim, and S. B. Choi, "Design of self-energizing clutch actuator for dual-clutch transmission," *IEEE/ASME Transactions on Mechatronics*, vol. 21, no. 2, pp. 795–805, 2015.
- [17] D.-H. Kim, J.-W. Kim, and S. B. Choi, "Design and modeling of energy efficient dual clutch transmission with ball-ramp self-energizing mechanism," *IEEE Transactions on Vehicular Technology*, vol. 69, no. 3, pp. 2525–2536, 2019.
- [18] D.-H. Kim and S. B. Choi, "Design of ball-ramp dual clutch transmission to reduce uncertainties in clutch actuator and tie-up effect," *Mechanism and Machine Theory*, vol. 176, p. 104982, 2022.
- [19] J. J. Oh and S. B. Choi, "Real-time estimation of transmitted torque on each clutch for ground vehicles with dual clutch transmission," *IEEE/ASME Transactions on Mechatronics*, vol. 20, no. 1, pp. 24–36, 2014.
- [20] J. J. Oh, J. S. Eo, and S. B. Choi, "Torque observer-based control of self-energizing clutch actuator for dual clutch transmission," *IEEE*

Transactions on Control Systems Technology, vol. 25, no. 5, pp. 1856–1864, 2016.

- [21] J. Kim, J. Oh, and S. B. Choi, “Nonlinear estimation method of a self-energizing clutch actuator load,” in *2012 First International Conference on Innovative Engineering Systems*. IEEE, 2012, pp. 231–236.
- [22] W.-H. Chen, D. J. Ballance, P. J. Gawthrop, and J. O’Reilly, “A nonlinear disturbance observer for robotic manipulators,” *IEEE Transactions on Industrial Electronics*, vol. 47, no. 4, pp. 932–938, 2000.
- [23] W.-H. Chen, “Disturbance observer based control for nonlinear systems,” *IEEE/ASME transactions on mechatronics*, vol. 9, no. 4, pp. 706–710, 2004.
- [24] K.-S. Kim, K.-H. Rew, and S. Kim, “Disturbance observer for estimating higher order disturbances in time series expansion,” *IEEE Transactions on automatic control*, vol. 55, no. 8, pp. 1905–1911, 2010.
- [25] S. Li, J. Yang, W.-H. Chen, and X. Chen, *Disturbance observer-based control: methods and applications*. CRC press, 2014.
- [26] D.-H. Kim and S. B. Choi, “Clutch torque estimation of ball-ramp dual clutch transmission using higher order disturbance observer,” in *2020 20th International Conference on Control, Automation and Systems (ICCAS)*. IEEE, 2020, pp. 743–749.
- [27] C.-Y. Cho, J.-H. Kam, H.-K. Hong, and C. Lövenich, “More efficiency with the dry seven-speed dual-clutch transmission by hyundai,” *ATZ worldwide*, vol. 118, no. 6, pp. 38–41, 2016.
- [28] J. Park, S. Choi, J. Oh, and J. Eo, “Adaptive torque tracking control during slip engagement of a dry clutch in vehicle powertrain,” *Mechanism and Machine Theory*, vol. 134, pp. 249–266, 2019.
- [29] S. Kim and S. Choi, “Control-oriented modeling and torque estimations for vehicle driveline with dual-clutch transmission,” *Mechanism and Machine Theory*, vol. 121, pp. 633–649, 2018.
- [30] K. Kong and M. Tomizuka, “Nominal model manipulation for enhancement of stability robustness for disturbance observer-based control systems,” *International Journal of Control, Automation and Systems*, vol. 11, no. 1, pp. 12–20, 2013.



Dong-Hyun Kim received the B.S. degree in mechanical engineering from Pusan National University, Busan, Korea, in 2016, the M.S. degree in mechanical engineering from the Korea Advanced Institute of Science and Technology (KAIST), Daejeon, Korea in 2018, and the Ph.D. degree in mechanical engineering from KAIST, in 2022. Since 2022, he has been with the senior research engineer of the Hyundai Motor Company. His research interests

development based on electric vehicle and vehicle motion control of electric vehicle.



Seibum B. Choi received the B.S. degree in mechanical engineering from Seoul National University, Seoul, Korea, in 1985, the M.S. degree in mechanical engineering from the Korea Advanced Institute of Science and Technology (KAIST), Daejeon, Korea in 1987, and the Ph.D. degree in control from the University of California, Berkeley, CA, USA, in 1993. From 1993 to 1997, he was involved in the development of automated vehicle control systems at the Institute of Transportation Studies, University of California. During 2006, he was with TRW, Warren,

MI, USA, where he was involved in the development of advanced vehicle control systems. Since 2006, he has been with the faculty of the Mechanical Engineering Department, KAIST. His current research interests include fuel-saving technology, vehicle dynamics and control, and active safety systems.